Microscopic structure of deformed and superdeformed collective bands in rotating nuclei

J. Kvasil,[1] N. Lo Iudice,[2] F. Andreozzi,[2] F. Knapp,[1] and A. Porrino[2]

[1]*Institute of Particle and Nuclear Physics, Charles University, V. Holešovičkách 2, CZ-18000 Praha 8, Czech Republic*

[2]*Dipartimento di Scienze Fisiche, Universitá di Napoli "Federico II" and Istituto Nazionale di Fisica Nucleare, Monte S. Angelo, Via Cintia I-80126 Napoli, Italy*

(Received 4 January 2007; published 15 March 2007)

We investigate in self-consistent cranked Nilsson plus quasiparticle random-phase approximation the structure of ^{190,192,194}Hg in their evolution from normal to superdeformation and from low to high rotational frequencies. The analysis of the energy levels suggests a splitting of few normally deformed bands into two or more branches. The investigation of the dynamical moments of inertia supports the octupole character of the low-lying negative parity superdeformed bands, in agreement with previous theoretical predictions and experimental findings. As a more direct confirm of their octupole nature, we obtain strong $E1$ transitions linking those bands to the yrast superdeformed band, in agreement with experiments. A similar result is shown to hold also for ^{152}Dy. Like in ^{152}Dy, the collectivity of the low-lying scissors mode gets enhanced with the onset of superdeformation.

DOI: 10.1103/PhysRevC.75.034306 PACS number(s): 21.60.Jz, 05.70.Fh, 27.80.+w, 27.70.+q

I. INTRODUCTION

The new generation of γ detectors is producing a growing mass of data on high-spin spectroscopy that allows a deeper understanding of the structure of nuclei under extreme conditions of fast rotation and superdeformation. The role of single-particle motion in determining the superdeformed (SD) minima, thereby generating new shell gaps, is well established [1,2]. The same single-particle model provides the key interpretation scheme for the quadrupole moments and the dynamical moments of inertia and their rotational evolution in nuclei of the $A \sim 150$ region [3–7].

According to most calculations, the SD minima in both $A \sim 152$ and $A \sim 190$ regions are soft toward octupole deformation [8–18] because of the presence of $\Delta l = 3$ intruder states in the region of Fermi surface. It is therefore natural to expect octupole fluctuations around SD minima. This was indeed predicted in a cranked Nilsson plus quasiparticle random-phase approximation (QRPA) for ^{152}Dy [19] and ^{190,192,194}Hg [20]. The calculation could reproduce the empirical dynamical moments of inertia in their rotational evolution thus supporting the prevalent role of octupole correlations in low-lying excited SD bands.

A more direct evidence in favor of octupole collectivity in SD nuclei was provided by several experiments on ^{190}Hg [21–25] and ^{194}Hg [26,27]. The experiments on ^{190}Hg measured strong $E1$ transitions connecting the excited SD2 to the yrast SD band. Those on ^{194}Hg not only measured fast $E1$ deexcitations of low-lying SD levels to the yrast SD band but were even able to measure their absolute energies and to observe transitions from SD to normally deformed (ND) levels.

Very similar results were obtained more recently on ^{152}Dy [28], where the SD6 band was found to deexcite to the yrast SD band via strong $E1$ transitions. The same experiment, combined with a previous one that linked the yrast SD band to ND states [29], could provide the absolute energy of the levels of the SD6 band.

In a recent work [30], we studied the octupole properties of SD bands in ^{152}Dy adopting a cranked Nilsson plus QRPA similar to the one used in Refs. [19,20]. We found similar fluctuations, in the rotational frequency, of the dynamical moment of inertia induced by octupole vibrations. We also studied how high-spin and superdeformation affect the electric multipole ($E\lambda$) giant resonances and the magnetic dipole ($M1$) mode.

The low-lying $M1$ mode came out to be of special relevance to possible future experiments. Because of the combined action of fast rotation and superdeformation, the orbital $M1$ strength gets so enhanced as to confer to the low-energy $M1$ excitations a dominant scissorslike character [31–33]. Such a feature was made explicit by the close link shown to exist between the $M1$ response and the kinematical moment of inertia in their evolution with rotation and deformation. That superdeformation deeply affects the scissors mode was established long ago [34]. Recent investigations using the same formalism as in Ref. [30] had emphasized the large impact of fast rotation on orbital $M1$ excitations [35].

The data presented in Ref. [28] on the the $E1$ transitions linking the SD6 to the yrast band of ^{152}Dy were not discussed in Ref. [30]. Although published earlier, Ref. [28] had escaped our attention. We present here our findings on this band jointly with the study of ND and SD rotational bands in ^{190,192,194}Hg.

Adopting the approach used in Ref. [30], we investigate how the collective properties of ^{190,192,194}Hg change as these nuclei rotate with increasing angular velocities and evolve from a ND to a SD shape. We focus our attention first on the octupole collectivity by showing how the negative parity bands change with rotation and how these changes affect the dynamical moment of inertia. For a more direct test of these correlations, we analyze the $E1$ transitions linking the excited SD bands to the yrast SD band. We also include in our study the SD6 band in ^{152}Dy and the $E1$ transitions connecting its levels to the yrast SD band.

 ©2007 The American Physical Society

We finally investigate how superdeformation plus rotation modify the structure of other collective modes, well established at normal deformation and low rotational frequency. We will check, in particular, if the enhancement of the collectivity of the low-lying scissors $M1$ mode with the onset of superdeformation, predicted for ^{152}Dy, is confirmed also for the Hg isotopes.

II. THEORETICAL FRAMEWORK

The cranked shell model plus RPA was developed long ago [36] and applied extensively to high-spin collective modes [37–46].

Following the procedure adopted in Refs. [30,35] we start with the Hamiltonian

$$H_\Omega = H_0(\Omega) + V_{\rm pair} + V_{\rm FF}, \tag{1}$$

where $V_{\rm pair}$ is a proton-proton and neutron-neutron monopole pairing, $V_{\rm FF}$ a sum of isoscalar and isovector separable potentials, and $H_0(\Omega)$ a cranked one-body term

$$H_0(\Omega) = H_0 - \sum_{\tau=n,p} \lambda_\tau N_\tau - \hbar\Omega I_1. \tag{2}$$

H_0 is a modified triaxial harmonic oscillator (HO) Nilsson Hamiltonian plus a local Galilean invariance restoring piece of the form given in Refs. [20,35,47], the second piece provides a constraint in the neutron and proton numbers, and the third is the cranking term.

The equilibrium deformation may be determined by minimizing at each Ω the expectation value of the above one-body Hamiltonian with respect to the HO frequencies ω_i, also dependent on Ω, under the volume conserving constraint

$$\omega_1\omega_2\omega_3 = \omega_0^3. \tag{3}$$

This prescription is equivalent to a Hartree mean-field approximation applied to a system of nucleons interacting via many-body forces [48,49].

The two-body potential is composed of several separable pieces

$$V = \sum_{\lambda\mu} \kappa_\lambda F''^2_{\lambda\mu}. \tag{4}$$

The sum includes quadrupole-quadrupole plus monopole-monopole plus spin-spin separable potentials, acting in the positive parity sector, as well as dipole-dipole plus octupole-octupole interactions, effective in the negative-parity subspace.

All multipole and spin-multipole fields $F''_{\lambda\mu}$ have good isospin T and signature, denoted by $r = \pm$ or, equivalently, $\alpha = 0, 1$ [50]. The fields are expressed in terms of doubly stretched coordinates $x''_i = (\omega_i/\omega_0)x_i$ [51,52]. These new variables guarantee, at least for a pure HO one-body Hamiltonian, that the self-consistent conditions

$$\langle Q''_\mu \rangle = 0, \quad \mu = 0, 1, 2 \tag{5}$$

be fulfilled for the quadrupole field at the equilibrium deformation, making feasible the separation of the spurious from the physical RPA solutions.

We express the Hamiltonian (1) in terms of quasiparticle creation and annihilation operators obtained through a Bogoliubov transformation and plug the transformed Hamiltonian into the RPA equations of motion

$$\begin{aligned} [H_\Omega, P_\nu] &= i\hbar\omega_\nu^2 X_\nu, \quad [H_\Omega, X_\nu] = -i\hbar P_\nu, \\ [X_\nu, P_{\nu'}] &= i\hbar\delta_{\nu\nu'}, \end{aligned} \tag{6}$$

where X_ν, P_ν are, respectively, the collective coordinates and their conjugate momenta.

The above RPA eigenvalue equations are solved separately for the positive and negative signature pieces, $H_\Omega(+)$ and $H_\Omega(-)$, respectively, under the constraints [35]

$$\begin{aligned} \left[H_\Omega(^{\pi=+}_{r=+}), N_\tau\right] &= 0, \quad \left[H_\Omega(^{\pi=-}_{r=+}), P_1\right] = 0, \\ \left[H_\Omega(^{\pi=+}_{r=+}), I_1\right] &= 0, \quad \left[H_\Omega(^{\pi=+}_{r=-}), \Gamma^\dagger\right] = \Omega\Gamma^\dagger, \end{aligned} \tag{7}$$

where

$$\Gamma^\dagger = \frac{1}{\sqrt{2\langle I_1\rangle}}(I_2 + iI_3) \tag{8}$$

and

$$\Gamma = (\Gamma^\dagger)^\dagger = \frac{1}{\sqrt{2\langle I_1\rangle}}(I_2 - iI_3) \tag{9}$$

satisfy the commutation relation

$$[\Gamma, \Gamma^\dagger] = 1. \tag{10}$$

The first three Eqs. (7) generate three Goldstone modes of positive signature, associated, respectively, with the nonconservation of the particle number induced by the Bogoliubov transformation and the breaking of translational and spherical symmetries of the mean field. The last equation yields a negative signature Goldstone mode. This, however, acquires a rotational energy $\omega_\lambda = \Omega$ from the cranking term responsible for breaking axial symmetry.

Equations (7) guarantee a complete separation of spurious or redundant modes from the intrinsic solutions. They are satisfied if a self-consistent Hartree-Bogoliubov (HB) mean field is adopted. As shown in Ref. [30], however, all those constraints are fulfilled with a good accuracy also in our minimization procedure under the volume conserving condition (3).

The tool for investigating the electromagnetic properties is represented by the strength function

$$S_{X\lambda}(E) = \sum_{\nu I'} B(X\lambda, I \to I', \nu)\delta(E - \hbar\omega_\nu), \tag{11}$$

where $B(X\lambda, I \to I', \nu)$ is the reduced strength of an electric ($X = E$) or magnetic ($X = M$) transition of multipolarity λ from a state of the yrast line with angular momentum I.

Because it is practically impossible to expand the cranked intrinsic RPA states into components with good K quantum numbers, the strength function is to be computed approximately in the limits of zero and high angular frequencies at the

shifted energy

$$S(E) \rightarrow S(E - \mu\hbar\Omega), \tag{12}$$

where $\mu = \Delta I = I - I_{\rm yrast}$, as required when moving from the intrinsic to the laboratory frame [39,40]. In these limits, the strength function can be computed efficiently by a method that avoids the explicit solution of the RPA eigenvalue equations, as long as the δ distribution is replaced by a Lorentzian weight [50].

Once the strength has been computed, it is straightforward to evaluate the $m_0(X\lambda)$ and $m_1(X\lambda)$ moments giving, respectively, the energy unweighted and weighted summed strengths by the formula

$$m_n(X\lambda) = \int_0^\infty E^n S_{X\lambda}(E) dE \tag{13}$$

valid for any nth moment.

III. MEAN-FIELD SOLUTIONS

Following Ref. [30], we determined the parameters of the Nilsson Hamiltonian by forcing such a Hamiltonian to reproduce at each Ω a set of single-particle energies close to the ones determined in a Nilsson-Strutinsky approach [53] and used in Ref. [2].

Such a fit yields, for the l^2 parameter μ, values considerably larger than the ones normally adopted [19,20,53]. As discussed in Ref. [30], however, these large values are only partly the results of our forced fit. Part of the discrepancy with respect to Refs. [19,20,53] is due to our use of *unstretched*, rather than *singly stretched*, coordinates in the Nilsson potential and to the coupling between all $\Delta N \neq 0$ shells fully accounted for here.

To avoid unwanted singularities in proximity of the critical frequencies, we have evaluated the pairing gaps following the phenomenological prescription [54]

$$\Delta_\tau(\Omega) = \begin{cases} \Delta_\tau(0)\left[1 - \frac{1}{2}\left(\frac{\Omega}{\Omega_c}\right)^2\right] & \Omega < \Omega_c \\ \Delta_\tau(0)\frac{1}{2}\left(\frac{\Omega_c}{\Omega}\right)^2 & \Omega > \Omega_c, \end{cases} \tag{14}$$

where Ω_c is the critical rotational frequency of the first band crossing. The pairing gaps at zero rotational frequency were deduced from the odd-even mass differences and resulted to be $\Delta_n(0) = 0.792$ MeV and $\Delta_p(0) = 0.806$ MeV for ^{190}Hg, $\Delta_n(0) = 0.817$ MeV and $\Delta_p(0) = 0.803$ MeV for ^{192}Hg, and $\Delta_n(0) = 0.842$ MeV and $\Delta_p(0) = 0.800$ MeV for ^{194}Hg.

We determined the equilibrium deformations at each angular velocity by minimizing at each Ω the BCS expectation value of the cranked Nilsson Hamiltonian (2) plus the pairing potential. Very similar equilibrium deformations were also obtained from the self-consistent conditions (5)

$$\langle Q''_{2\mu}\rangle_\Omega = \langle\Omega|Q''_{2\mu}|\Omega\rangle = 0, \quad \mu = 0, 2 \tag{15}$$

at each Ω. As already pointed out, these zeros correspond to the energy minima of the HO Hamiltonian under the volume conserving constraint [48,49].

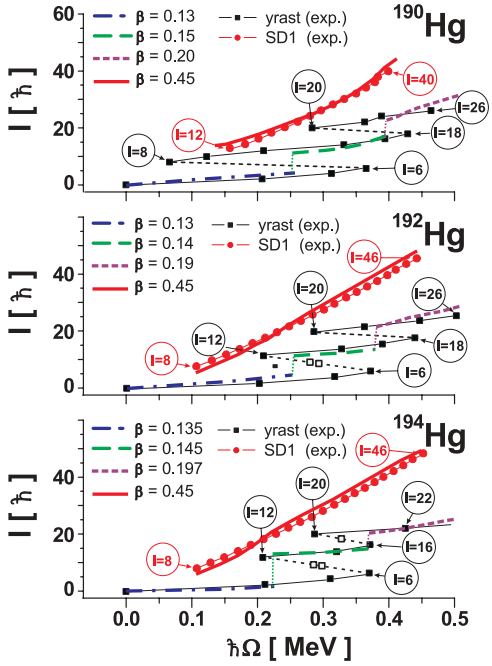

FIG. 1. (Color online) Angular momenta versus rotational frequency.

It must be pointed out that the energy minima are sensitive to the details of the Nilsson Hamiltonian and, in particular, to the l^2 term [55], whose effect here is amplified. However, we checked that the collective responses are little sensitive to these changes.

For all nuclei under investigation and all rotational frequencies, we obtained two minima, both axially symmetric ($\gamma = 0$). One of them is the SD minimum. It occurs at $\beta = 0.45$ and is insensitive to Ω. The other falls at low deformation ($\beta = 0.13 - 0.20$) and is weakly dependent on Ω. In ^{190}Hg, for instance, the minimum moves from $\beta = 0.13$ for $\Omega < 0.25$ MeV to $\beta = 0.15$ for $0.25 < \Omega < 0.40$ (MeV) and, further, to $\beta = 0.20$ for $\Omega > 0.40$ MeV. Each jump in deformation corresponds to a band crossing in turn connected with a backbending critical point.

The full picture is more vividly illustrated in Fig. 1, where the angular-momentum expectation value, $\langle I_x\rangle_\Omega = \langle\Omega|I_x|\Omega\rangle$ is plotted against the angular frequency. The plots show clearly for all three nuclei a close connection between β discontinuities and band crossings as well as the onset of first and second backbending. The substantial agreement of the theoretical lines with experimental points emphasizes the validity of our mean-field approach.

In all Hg isotopes, the ND minima are deeper than the SD ones at all frequencies. Consequently, the SD band is never yrast and, therefore, decays to the ND states. This is at variance with ^{152}Dy where the SD band becomes yrast starting from $\Omega \sim 0.6$ MeV.

IV. RPA ANALYSIS OF ND BANDS

The rotational spectrum of ^{190}Hg, as determined in Refs. [21,22,25] and reviewed in Ref. [56], is composed of 21 bands,

labeled $Bi = B1, \ldots B21$. Four of them, $B18, B19, B20, B21$, are superdeformed and are denoted as SD1, SD2, SD3, SD4, following a widely common practice. The energies of the SD bands with respect to the ND ones are not known. Few $E1$ transitions, connecting the SD2 to the yrast SD band (SD1), have been measured and the relative energies between the two bands determined.

The rotational bands observed so far in ^{192}Hg amount to 14 [57,58]. Three of them, $B9$, $B10$, $B11$, are superdeformed. The relative energies of the SD bands among themselves and with respect to ND bands are not known.

The experimental spectrum of ^{194}Hg has 15 rotational bands [59]. Among them, three ($B13$, $B14$, $B15$) are superdeformed. The energies of all of them with respect to the ND bands are also known.

As in Ref. [30], we solved the RPA Eqs. (6) under the symmetry constraints (7) for each parity and signature (π, α). It is important to enforce these constraints at each Ω. Only by doing so were we able to separate the redundant or spurious solutions from the physical ones at all rotational frequencies. The same constraints fixed the strength constants of the multipole-multipole interactions. The fact that these constants came out to be close to the HO values [35] reflects the essential self-consistent character of our approach. The strengths of the spin-spin interaction, the only ones left out, were fixed in the standard way [35,60]. Finally, we used bare charges for the $E\lambda$ transitions and a quenching factor $g_s = 0.7$ for the spin gyromagnetic ratios.

The experimental Routhians $R_\nu[\Omega_\nu(I)]$ were extracted from the observed energy levels $E_\nu(I)$ of each rotational band ν through the standard formula

$$R_\nu[\Omega_\nu(I)] = E_\nu(I) - \hbar\Omega_\nu(I)I, \tag{16}$$

where the rotational frequency is given by

$$\hbar\Omega_\nu(I) = \frac{E_\nu(I+2) - E_\nu(I)}{2}. \tag{17}$$

The RPA energies $\hbar\omega_\nu$ were compared with the differences $R_\nu(\Omega_\nu) - R_{\text{yrast}}(\Omega_\nu)$. This was done for the ND levels of given parity and signature shown in Figs. 2–4.

The $B14$ and $B15$ bands in ^{190}Hg and the $B13$ and $B14$ bands in ^{192}Hg did not fit into the signature classification scheme. Each of these bands was therefore split into two, one with positive $(\pi, \alpha = 0)$ and the other with negative $(\pi, \alpha = 1)$ signatures. Thus, the negative-parity band $B14$ was decomposed into the $(\pi, \alpha = 0)$ $B14a$ and the $(\pi, \alpha = 1)$ $B14b$ bands.

Moreover, groups of levels, though belonging to the same band, yield moments of inertia and Routhians very different from each other. This is the case of the bands $B14a$, $B14b$ in ^{190}Hg, $B14b$ in ^{192}Hg, and $B10$ in ^{194}Hg. Thus, we suggest that each of these bands should split into two branches, each with alike moments of inertia and Routhians. These branches are labeled as $B14a1$, $B14a2$ and so on.

Figures 2–4 show that all ND bands fit fairly well into the RPA level scheme. Following the evolution of the levels with Ω, one may notice, in the positive-parity and signature

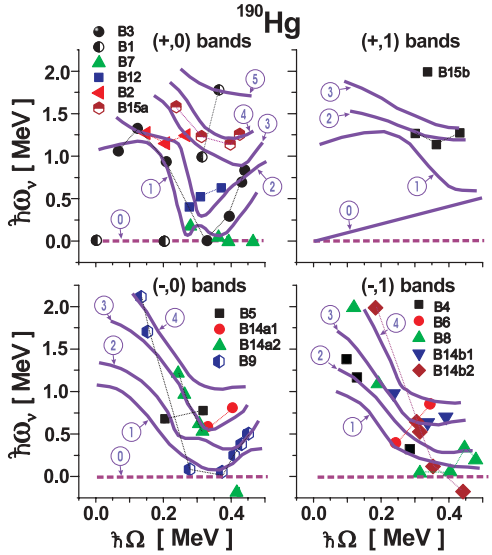

FIG. 2. (Color online) RPA and experimental spectra at different angular velocities in ^{190}Hg.

(+, 0) plot, the rapid downfall of RPA levels in correspondence of the experimental level crossings connected with the first and second backbending. One may also notice the rapid decrease with Ω of the negative-parity bands. The difference between experimental Routhian becomes negative even for the $B14b2$ band of ^{190}Hg and the $B7$ and $B14b2$ bands of ^{192}Hg. This means only that the positive-parity ND band is no longer the yrast band, thus reflecting instability toward octupole deformation. Our mean-field approach is clearly not adequate to describe these bands. It should be necessary to modify the one-body potential so as to incorporate octupole deformations.

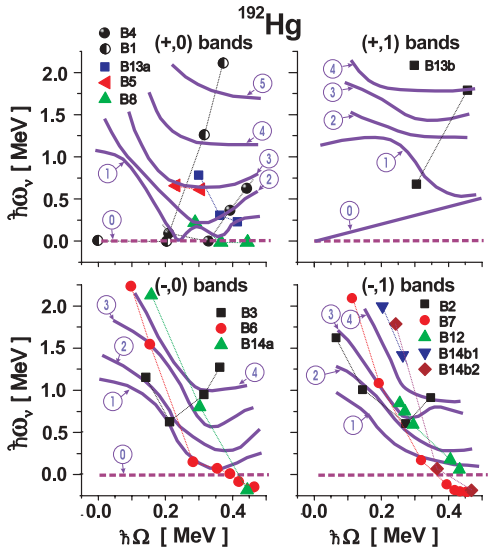

FIG. 3. (Color online) RPA and experimental spectra at different angular velocities in ^{192}Hg.

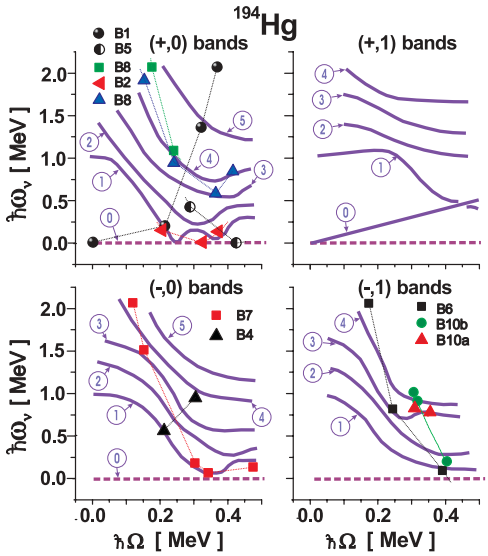

FIG. 4. (Color online) RPA and experimental spectra at different angular velocities in ^{194}Hg.

V. RPA ANALYSIS OF SD BANDS

A. Energies and dynamical moment of inertia

To investigate the superdeformed bands we solved the RPA Eqs. (6) on top of the secondary superdeformed minimum. The eigenvalues were compared with the difference of Routhians $R_\nu(\Omega) - R_{\rm SD1}(\Omega)$, where SD1 is the lowest SD yrast band. The low-lying RPA SD levels are plotted in Fig. 5. The agreement with the available experimental data is good.

The calculation confirms the close link, predicted in Ref. [20], of the low-lying negative-parity SD levels with the octupole degrees of freedom. This link was found also in ND bands at high Ω.

Another point worthy of attention is the crossing of the lowest two negative-parity SD bands of both signatures in ^{190}Hg and ^{192}Hg but not in ^{194}Hg. These crossings induce

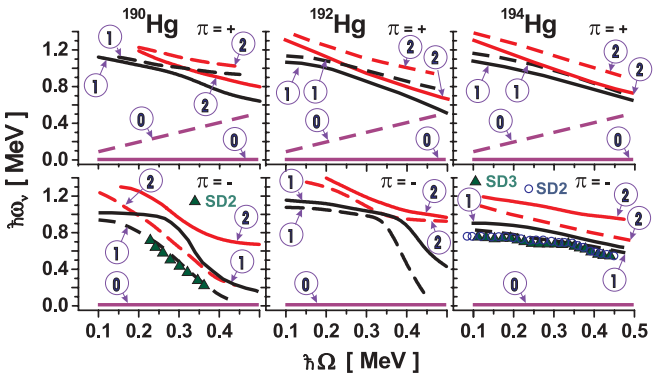

FIG. 5. (Color online) Rotational evolution of the RPA energies of the lowest positive ($\pi = +$) and negative ($\pi = -$) parity SD bands in ^{190,192,194}Hg. Full and dashed lines correspond to positive ($\alpha = 0$) and negative ($\alpha = 1$) signatures, respectively. The corresponding experimental levels are denoted by circles ($\alpha = 0$) and triangles ($\alpha = 1$). The data are taken from Refs. [21,22,25] for ^{190}Hg and from [26,57] for ^{194}Hg.

large fluctuations on the dynamical moment of inertia. This was computed using the formula

$$\Im^{(2)}_\nu(\Omega) = \Im^{(2)}_{\rm yr} - \frac{d^2 E_\nu}{d\Omega^2}, \tag{18}$$

where $\Im^{(2)}_{\rm yr}$ is the dynamical moment of inertia of the SD yrast band, given approximately by the Harris formula

$$\Im^{(2)}_{\rm yr} = a + b\Omega^2 + c\Omega^4. \tag{19}$$

From the fit of the SD1 band we extracted the parameters $a = 82.6\hbar^2\,{\rm MeV}^{-1}$, $b = 339\hbar^2\,{\rm MeV}^{-3}$, and $c = 0\hbar^2\,{\rm MeV}^{-5}$ in ^{190}Hg, $a = 91.7\hbar^2\,{\rm MeV}^{-1}$, $b = 264.6\hbar^2\,{\rm MeV}^{-3}$, and $c = 0\hbar^2\,{\rm MeV}^{-5}$ in ^{192}Hg, and $a = 88.5\hbar^2\,{\rm MeV}^{-1}$, $b = 339\hbar^2\,{\rm MeV}^{-3}$, and $c = -195\hbar^2\,{\rm MeV}^{-5}$ in ^{194}Hg.

The fluctuating part, given by the second derivative of the RPA energy $E_\nu(\Omega) = (\hbar\omega)_\nu(\Omega)$, was computed for a given band at different rotational frequencies. The theoretical moment of inertia (18), computed following the above prescriptions, was compared with the empirical one. This was extracted from the levels of each rotational band according to

$$\Im^{(2)}_\nu(\Omega) = \hbar\frac{dI}{d\Omega_\nu} = \frac{4\hbar^2}{E_\nu(I+4) - 2E_\nu(I+2) - E_\nu(I)}. \tag{20}$$

As shown in Fig. 6, the dynamical moment of inertia undergoes strong variations with Ω only in the $(-,0)$SD4 band in ^{190}Hg and the $(-,1)$SD2 and $(-,0)$SD3 bands in ^{192}Hg. All these bands display a crossing of the two lowest

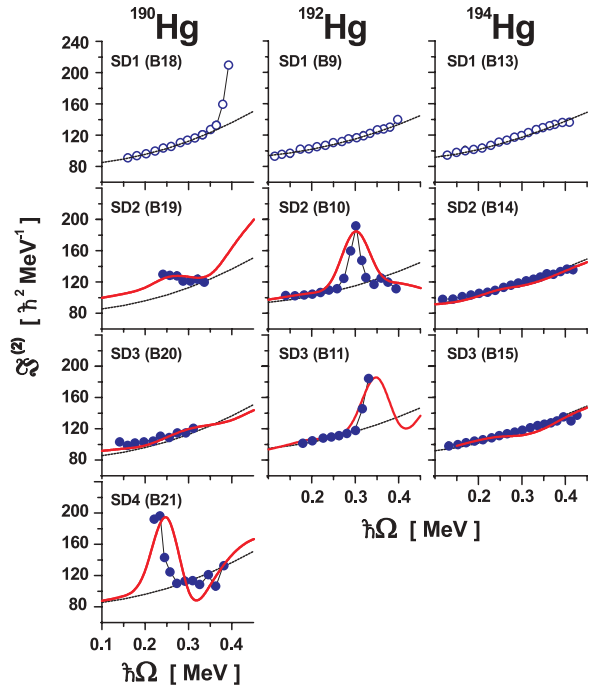

FIG. 6. (Color online) The dynamical moments of inertia, determined by Eq. (18) (solid lines), is compared to the corresponding empirical values obtained from Eq. (20). The dotted lines give the Harris fit [Eq. (19)].

TABLE I. Strengths of the $E1$ transitions from the SD2 to the yrast SD band in ^{190}Hg.

$J_i^\pi \to J_f^\pi$	E_γ (keV)	$B(E1)_{\rm exp}$ (W.u.)	$B(E1)_{\rm th}$ (W.u.)
$25^- \to 24^+$	911	$>1.4 \times 10^{-3}$[a]	2.29×10^{-3}
$27^- \to 26^+$	864	$1.2(3) \times 10^{-3}$[a]	1.58×10^{-3}
		$3.8(8) \times 10^{-3}$[b]	
$29^- \to 28^+$	812	$1.5(4) \times 10^{-3}$[a]	0.99×10^{-3}
		$1.5(3) \times 10^{-3}$[b]	
$31^- \to 30^+$	757	$<2.4 \times 10^{-3}$[a]	1.62×10^{-3}
		$1.6(4) \times 10^{-3}$[b]	

[a]Taken from Ref. [22].
[b]Taken from Ref. [25].

bands, as already pointed out. This crossing yields nonzero second derivatives of the energy in Eq. (18) and, therefore, is responsible for the fluctuations of the moments of inertia with Ω, in fairly good agreement with the experiments.

In all other bands, including all SD bands of ^{194}Hg, both theoretical and empirical moments of inertia vary smoothly with Ω.

B. $E1$ transitions among low-lying SD bands

A more direct test of the collective properties of rotational and superdeformed bands comes from the measurement of electromagnetic transition strengths. The experimental information on these properties is still rather scant.

Recent experiments, however, have identified few $E1$ transitions linking the excited SD2 band to the yrast SD band in ^{190}Hg [25] and measured the $E1$ decay strengths. Also in ^{194}Hg few relatively strong $E1$ transitions connecting the SD3 to the yrast SD band were identified [26]. Table I shows measured and computed $E1$ transition strengths from the SD2 to the yrast SD band in ^{190}Hg. The agreement is quite satisfactory, stressing once more the important role of octupole correlations in this band.

For the not-yet-measured $E1$ transitions linking the SD4 band to the yrast SD1 band in ^{190}Hg we found $B(E1, I^-\text{SD4} \to I^+\text{SD1}) \simeq 3 \times 10^{-3}$ W.u. at $\Omega \sim 0.2$ MeV and the smaller values $B(E1, I^-\text{SD4} \to I^+\text{SD1}) \simeq 0.5 \times 10^{-3}$ W.u. for $\Omega \sim 0.4$. Similar results hold for the unmeasured $E1$ strengths in ^{192}Hg. We got for both SD2 and SD3 bands $B(E1, I^- \to I^+\text{SD1}) \simeq 2.5 \times 10^{-3}$ W.u. at $\Omega \sim 0.2$ MeV $B(E1, I^- \to I^+\text{SD1}) \simeq 10^{-4}$ W.u. at $\Omega \sim 0.4$ MeV. It seems that the admixture of $K^\pi = 1^-$ and $K^\pi = 0^-$ octupole amplitudes decreases as Ω increases, in agreement with the conclusions drawn in Refs. [20,26].

As shown in Table II, the computed strengths of few $E1$ transitions, connecting the SD3 to the yrast SD band in ^{194}Hg, agree qualitatively with the rough estimates given in Ref. [26], confirming the octupole nature of the band. These $E1$ strengths are smaller than in ^{190,192}Hg and, contrary to the latter isotopes, are little affected by rotation. In fact, we obtained $B(E1, I^-\text{SD2} \to I^+\text{SD1}) \simeq 10^{-4}$ W.u. at all Ω's.

TABLE II. Strengths of the $E1$ transitions from the SD3 to the yrast SD band in ^{194}Hg. The experimental values are reported to be of the order of $\sim 10^{-5}$ W.u. for all $E1$ transitions [26].

$J_i^\pi \to J_f^\pi$	E_γ (keV)	$B(E1)_{\rm th}$ (W.u.)
$11^- \to 10^+$	824.2	0.92×10^{-4}
$13^- \to 12^+$	832.4	1.12×10^{-4}
$15^- \to 14^+$	839.1	0.83×10^{-4}
$17^- \to 16^+$	844.6	0.72×10^{-4}
$19^- \to 18^+$	848.8	0.91×10^{-4}

The quenching of the $E1$ transitions in ^{194}Hg compared to ^{190,192}Hg combined with the absence of level crossing and the ensuing smooth behavior of the moment of inertia may be explained with the fact that the SD bands in ^{194}Hg keep their $K = 2$ character and contain smaller $K = 0, 1$ components [20,27].

VI. A SHORT ANALYSIS OF THE SD6 BAND IN ^{152}DY

To complete the study of the collective properties of rotational spectra in ^{152}Dy performed in Ref. [30], we computed all quantities that characterize the SD6 band and compared our results with the experimental data [28].

As shown in Fig. 7, the QRPA SD6 energy follows closely, though remaining few keV below, the measured energy in its Ω path. Our QRPA values are very similar to the ones obtained in Ref. [20]. We can therefore state that our calculation supports

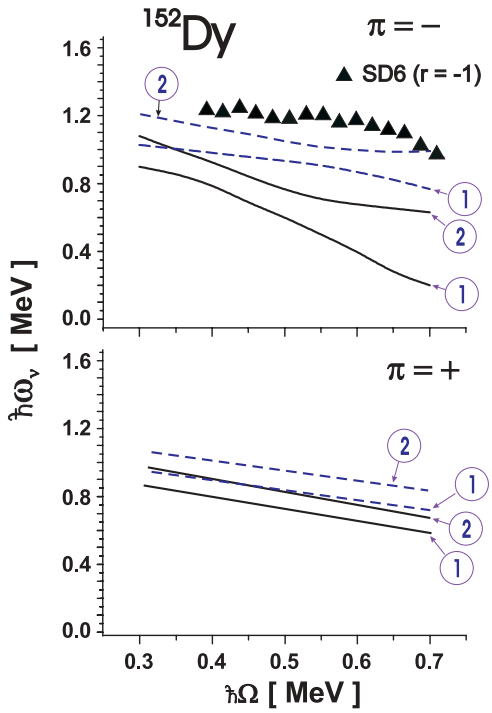

FIG. 7. (Color online) Evolution with the rotational frequency Ω of the energy of the SD6 band in ^{152}Dy. The experimental data are taken from Ref. [28].

TABLE III. Strengths of the $E1$ transitions from the SD6 to the yrast SD band in ^{152}Dy. The experimental data are taken from Ref. [28].

$J_i^\pi \to J_f^\pi$	E_γ (keV)	$B(E1)_{\rm exp}$ (W.u.)	$B(E1)_{\rm th}$ (W.u.)
$33^- \to 32^+$	1676	2.2×10^{-4}	2.86×10^{-4}
$35^- \to 34^+$	1696	3.8×10^{-4}	1.86×10^{-4}
$37^- \to 36^+$	1715	4.5×10^{-4}	1.94×10^{-4}
$39^- \to 38^+$	1734	3.9×10^{-4}	1.74×10^{-4}
$41^- \to 40^+$	1751	4.9×10^{-4}	3.69×10^{-4}

the interpretation of the SD6 band as an octupole vibrational band.

This interpretation is strengthened by the analysis of the $E1$ transitions linking the SD6 levels to the yrast SD band. As shown in Table III, the computed $E1$ strengths are generally smaller than the experimental ones by at most a factor of 2. Such a substantial agreement supports strongly the prevalence of the octupole degree of freedom in such a band.

VII. GIANT RESONANCES AND $M1$ MODE

The electromagnetic response in the Hg isotopes is similar to the one in ^{152}Dy [30]. As shown in Fig. 8, the $E1$ giant resonance built on the SD minimum gets damped and splits into too broad peak, a $K^\pi = 0^-$ prominent one around 10–11 MeV and a smaller peak around 21–22 MeV.

In Fig. 9, the strong $E0$ peak remains at about 16 MeV for small deformations and slow rotations. It spreads and shifts at about 20 MeV with the onset of superdeformation. Moreover,

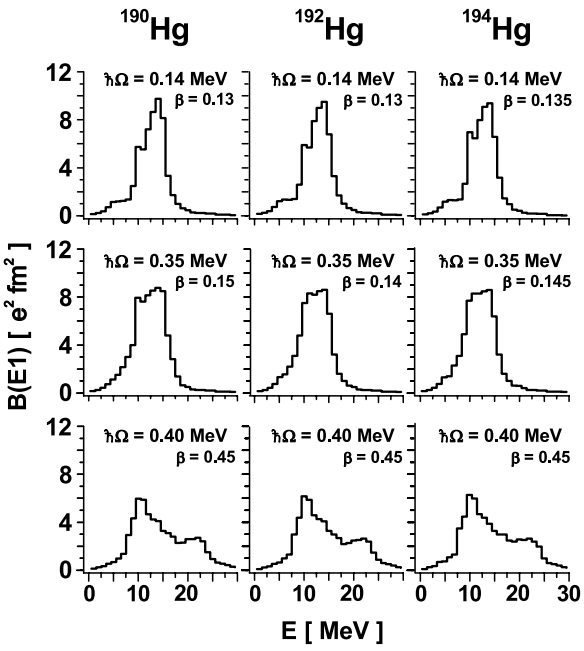

FIG. 8. $E1$ strength distribution for different angular frequencies and deformations. The reduced strengths are summed in bins of 1 MeV around the energy E of the final state excited from the yrast band.

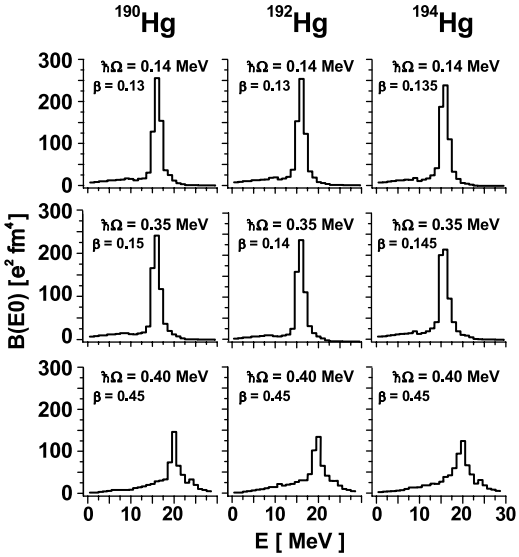

FIG. 9. $E0$ spectra for different angular frequencies and deformations. The reduced strengths are summed in bins as in Fig. 8.

the structure of the $E2$ giant resonance is substantially altered only at high rotational frequencies and superdeformation (Fig. 10). The small high-energy isovector peak is swept away, whereas the low- and high-energy branches of the isoscalar resonance get damped and spread over a wider energy range.

As in ^{152}Dy, the $M1$ response changes qualitatively in going from the ND to the SD phase (Fig. 11). At normal deformation, most of the $M1$ strength is concentrated within the energy range of $2 \div 10$ MeV, peaks around 5–6 MeV, and is due mainly to spin excitations. Only in the low-energy tail $(2 \div 4)$ MeV are orbital and spin contributions comparable. The shape and structure of the peak remain unchanged even at relatively high rotational frequencies for small deformations.

With the onset of superdeformation, the strength gets enhanced at low as well as high energy. At low energy, the

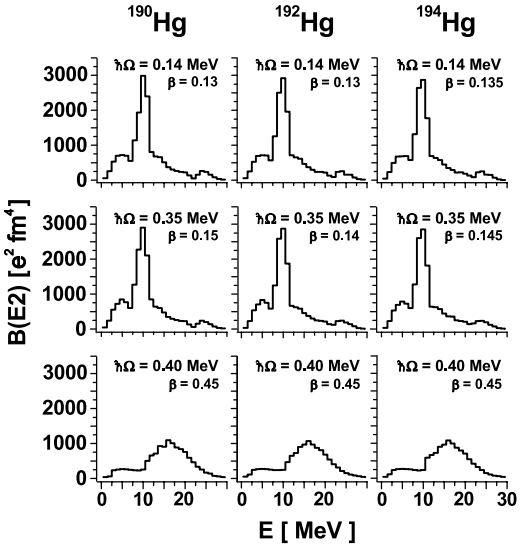

FIG. 10. $E2$ spectra for different angular frequencies and deformations. The reduced strengths are summed in bins as in Fig. 8.

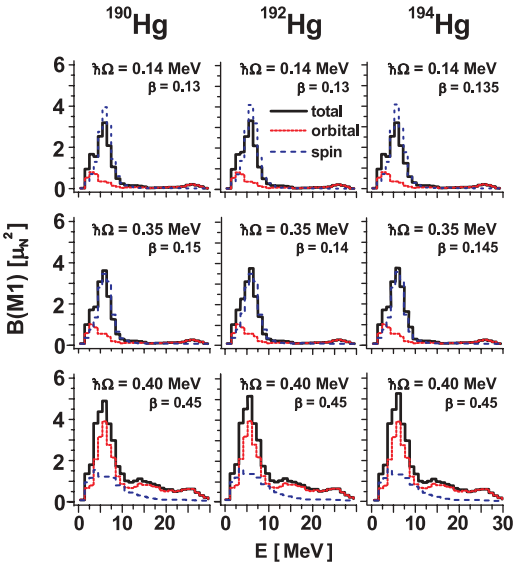

FIG. 11. (Color online) $M1$ spectra for different angular frequencies and deformations. The reduced strengths are summed in bins as in Fig. 8.

strength remains concentrated in the same $2 \div 10$ interval and still peaks around 5–6 MeV. The peak, however, is more prominent and dominated by the orbital motion. The orbital strength appears dominant over the whole energy range, whereas the spin transitions are quenched and scattered all along. It follows that the shape and peak of the total $M1$ strength distribution result to be determined mainly by the orbital response.

For a better characterization of the mode, we put the $m_1(M1)$ moment, yielding the energy weighted sum of the $M1$ strengths, in relation to the kinematical moment of inertia

$$\Im_\nu^{(1)}(\Omega) = \frac{\hbar I}{\Omega_\nu(I)} = \frac{2I\hbar^2}{E_\nu(I+2) - E_\nu(I)}. \qquad (21)$$

As shown in Fig. 12, the orbital $M1$ moment appears closely correlated with the moment of inertia as the system evolves. The dramatic enhancement induced by superdeformation is similar in both quantities. In virtue of a such a close link with $\Im^{(1)}$, we may safely state that the low-lying peak arises from the excitation of the scissors mode. For such a mode, indeed, the following energy weighted sum rule holds [61,62]

$$m_1(M1)^{(\mathrm{sc})} = \sum_n (E_n - E_0) B_n^{(\mathrm{sc})}(M1) = \frac{3}{16\pi} \Im^{(1)} \omega^2, \qquad (22)$$

where ω is the centroid of the scissorslike excitations.

Apart from the octupole mode, the $M1$ is the lowest collective mode in energy. Its detection might not be prohibitive with the new accelerators and detectors. Thanks to the recent technological improvements, a γ cascade experiment could disentangle the $M1$ from the $E\lambda$ deexcitations and provide evidence of a scissors mode built on excited states in slowly rotating nuclei [63].

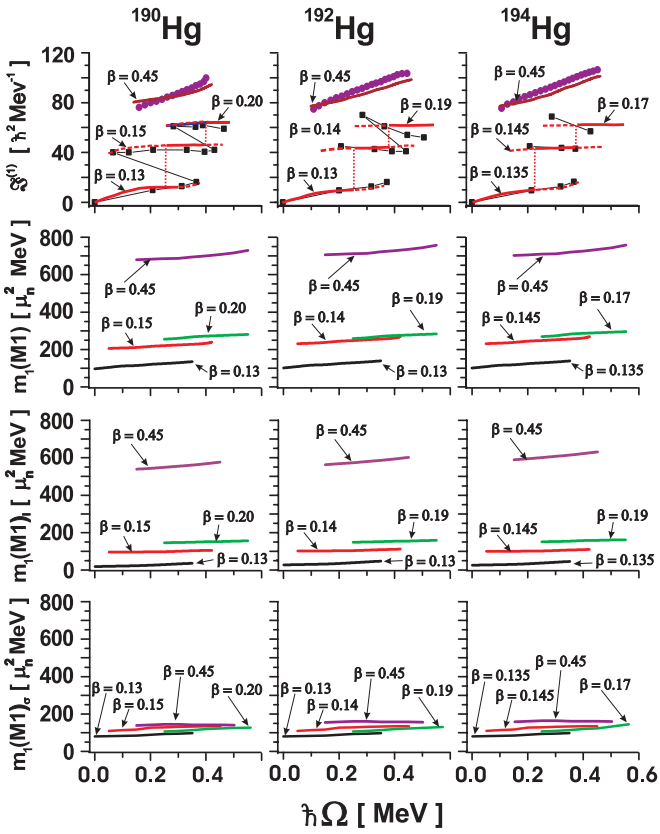

FIG. 12. (Color online) The yrast line kinematical moment of inertia (upper panel) versus the total (second panel), orbital (third panel), and spin (bottom panel) $m_1(M1)$ moments.

VIII. CONCLUSIVE REMARKS

A basically selfconsistent cranked Nilsson plus QRPA approach, previously adopted for ^{152}Dy, has proved to be successful also in describing the properties of the high-spin levels in ^{190,192,194}Hg.

It accounts fairly well for the dynamical moment of inertia all along their deformation and rotational paths, confirming the octupole character of the negative-parity excited SD bands near the yrast line, in agreement with previous predictions [19,20].

The approach accounts quantitatively well for the strong $E1$ transitions connecting the excited to the yrast SD bands, measured in ^{190,192,194}Hg [22,25,26] and in ^{152}Dy [28]. The deexcitation of these SD bands via strong $E1$ transitions is a more direct test of their octupole character.

A careful analysis of moments of inertia and Routhians has suggested a split of some ND bands into different branches according to signature and homogeneous moments of inertia. In our opinion, this point deserves a detailed experimental test.

Our analysis confirms the pronounced influence of superdeformation on all collective modes, just as in ^{152}Dy. In particular, we found that superdeformation greatly enhances the strength of the orbital $M1$ transitions to the point of conferring to the low-lying $M1$ excitations the typical features of the scissors mode. Being the lowest in energy, apart from the octupole excitations, such a mode may well be proposed for future experiments. p''

ACKNOWLEDGMENTS

We thank Drs. T. Lauritsen and R. V. F. Janssens for bringing to our attention their data on the $E1$ transitions in ^{152}Dy, which we overlooked during our earlier investigation on this nucleus. This work was partly supported by the Italian Ministero dell'Istruzione, Universitá and Ricerca (MIUR), the research plan MSM 0021620834 supplied by the Ministry of Education of the Czech Republic, the Charles University Grant Agency (grant 222/2006/B-FYZ/MFF), and the Czech Grant Agency (grant 202/06/0363).

[1] W. Nazarewicz, R. Wyss, and A. Johnson, Nucl. Phys. **A503**, 285 (1989).
[2] Y. R. Shimizu, E. Viggezi, and R. A. Broglia, Nucl. Phys. **A509**, 80 (1990).
[3] T. Bengtsson, I. Ragnarson, and S. Aberg, Phys. Lett. **B208**, 39 (1988).
[4] R. V. F. Janssens and T. L. Khoo, Annu. Rev. Nucl. Part. Sci. **41**, 321 (1991).
[5] W. Satula, J. Dobaczewski, J. Dudek, and W. Nazarewicz, Phys. Rev. Lett. **77**, 5182 (1996).
[6] L. B. Karlsson, I. Ragnarsson, and S. Aberg, Nucl. Phys. **A639**, 654 (1998).
[7] S. T. Clark *et al*., Phys. Rev. Lett. **87**, 172503 (2001).
[8] J. Dudek, T. R. Werner, and Z. Szymanski, Phys. Lett. **B248**, 235 (1990).
[9] J. Skalski, Phys. Lett. **B274**, 1 (1992).
[10] J. Skalski *et al*., Nucl. Phys. **A551**, 109 (1993).
[11] S. Mizutori, Y. R. Shimizu, and K. Matsuyanagi, Prog. Theor. Phys. **83**, 666 (1990).
[12] S. Mizutori, Y. R. Shimizu, and K. Matsuyanagi, Prog. Theor. Phys. **86**, 131 (1991).
[13] J. Höller and S. Aberg, Z. Phys. A **336**, 363 (1990).
[14] P. Bonche, S. J. Krieger, M. S. Weiss, J. Dobaczewski, H. Flocard, and P. H. Heenen, Phys. Rev. Lett. **66**, 876 (1991).
[15] X.-J. Li, J. Dudek, and P. Romain, Phys. Lett. **B271**, 281 (1991).
[16] T. Nakatsukasa, S. Mizutori, and K. Matsuyanagi, Prog. Theor. Phys. **87**, 607 (1992).
[17] R. Nazmitdinov and S. Aberg, Phys. Lett. **B289**, 238 (1992).
[18] J. Meyer *et al*., Nucl. Phys. **A588**, 597 (1995).
[19] T. Nakatsukasa, K. Matsuyanagi, S. Mizutori, and W. Nazarewicz, Phys. Lett. **B343**, 19 (1995).
[20] T. Nakatsukasa, K. Matsuyanagi, S. Mizutori, and Y. R. Shimizu, Phys. Rev. C **53**, 2213 (1996).
[21] B. Crowell *et al*., Phys. Lett. **B333**, 320 (1995).
[22] B. Crowell *et al*., Phys. Rev. C **51**, R1599 (1995).
[23] A. N. Wilson *et al*., Phys. Rev. C **54**, 559 (1996).
[24] H. Amro *et al*., Phys. Lett. **B413**, 15 (1997).
[25] A. Korichi *et al*., Phys. Rev. Lett. **86**, 2746 (2001).
[26] G. Hackman *et al*., Phys. Rev. Lett. **79**, 4100 (1997).
[27] P. Fallon *et al*., Phys. Rev. C **55**, R999 (1997).
[28] T. Lauritsen *et al*., Phys. Rev. Lett. **89**, 282501 (2002).
[29] T. Lauritsen *et al*., Phys. Rev. Lett. **88**, 042501 (2002).
[30] J. Kvasil, N. Lo Iudice, F. Andreozzi, F. Knapp, and A. Porrino, Phys. Rev. C **73**, 034302 (2006).
[31] N. Lo Iudice and F. Palumbo, Phys. Rev. Lett. **41**, 1532 (1978).
[32] D. Bohle, A. Richter, W. Steffen, A. E. L. Dieperink, N. Lo Iudice, F. Palumbo, and O. Scholten, Phys. Lett. **B137**, 27 (1984).
[33] For an exhaustive list of references see N. Lo Iudice, Rivista del Nuovo Cimento **23**, 1 (2000).
[34] I. Hamamoto and W. Nazarewicz, Phys. Lett. **B297**, 25 (1992).
[35] J. Kvasil, N. Lo Iudice, R. G. Nazmitdinov, A. Porrino, and F. Knapp, Phys. Rev. C **69**, 064308 (2004).
[36] E. R. Marshalek, Phys. Rev. C **11**, 1426 (1975); Nucl. Phys. **A266**, 317 (1976).
[37] J. L. Egido, H. J. Mang, and P. Ring, Nucl. Phys. **A339**, 390 (1980).
[38] Y. R. Shimizu and K. Matsuyanagi, Prog. Theor. Phys. **70**, 144 (1983); **72**, 799 (1984).
[39] P. Ring, L. M. Robledo, J. L. Egido, and M. Faber, Nucl. Phys. **A419**, 261 (1984).
[40] Y. R. Shimizu and K. Matsuyanagi, Prog. Theor. Phys. **75**, 1161 (1986).
[41] L. M. Robledo, J. L. Egido, and P. Ring, Nucl. Phys. **A449**, 201 (1986).
[42] S. Mizutori, Y. R. Shimizu, and K. Matsuyanagi, Prog. Theor. Phys. **83**, 666 (1990); **85**, 559 (1991); **86**, 131 (1991).
[43] T. Nakatsukasa, S. Mizutori, and K. Matsuyanagi, Prog. Theor. Phys. **87**, 607 (1992); **89**, 847 (1993).
[44] S. Mizutori, T. Nakatsukasa, K. Arita, Y. R. Shimizu, and K. Matsuyanagi, Nucl. Phys. **A557**, 125c (1993).
[45] T. Nakatsukasa, K. Matsuyanagi, S. Mizutori, and W. Nazarewicz, Phys. Lett. **B343**, 19 (1995).
[46] Y. R. Shimizu and K. Matsuyanagi, Nucl. Phys. **A588**, 559 (1995).
[47] J. Kvasil and R. G. Nazmitdinov, Phys. Rev. C **69**, 031304(R) (2004).
[48] E. R. Marshalek, Phys. Rev. Lett. **51**, 1534 (1983).
[49] E. R. Marshalek, Phys. Rev. C **29**, 640 (1984).
[50] J. Kvasil, N. Lo Iudice, V. O. Nesterenko, and M. Kopal, Phys. Rev. C **58**, 209 (1998).
[51] T. Kishimoto, J. M. Moss, D. H. Youngblood, J. D. Bronson, C. M. Rozsa, D. R. Brown, and A. D. Bacher, Phys. Rev. Lett. **35**, 552 (1975).
[52] H. Sakamoto and T. Kishimoto, Nucl. Phys. **A501**, 205 (1989).
[53] T. Bengtsson and I. Ragnarsson, Nucl. Phys. **A436**, 14 (1985).
[54] R. Wyss, W. Satula, and W. Nazarewicz, Nucl. Phys. **A511**, 324 (1990).
[55] Y. R. Shimizu and K. Matsuyanagi, Prog. Theor. Phys. **71**, 960 (1984).
[56] B. Singh, Nucl. Data Sheets **99**, 175 (2003); http://www.nudc.bnl.gov/
[57] P. Fallon *et al*., Phys. Rev. C **51**, R1609 (1995).
[58] C. M. Baglin, Nucl. Data Sheets **79**, 277 (1996); http://www.nudc.bnl.gov/
[59] E. Browne and B. Singh, Nucl. Data Sheets **79**, 277 (1996); http://www.nudc.bnl.gov/
[60] B. Castel and I. Hamamoto, Phys. Lett. **B65**, 27 (1976).
[61] E. Lipparini and S. Stringari, Phys. Lett. **B130**, 139 (1984).
[62] N. Lo Iudice, Phys. Rev. C **57**, 1246 (1998).
[63] M. Krticka, F. Becvar, J. Honzatko, I. Tomandl, M. Heil, F. Kappeler, R. Reifarth, F. Voss, and K. Wisshak, Phys. Rev. Lett. **92**, 172501 (2004).